2008 IEEE/RSJ International Conference on Intelligent Robots and Systems
Acropolis Convention Center
Nice, France, Sept, 22-26, 2008

Stable and Quick Standing–Sitting Motion of I-PENTAR by Whole-body Motion with Force Control

SeongHee JEONG and Takayuki TAKAHASHI

Abstract— **This paper describes motion control and planning for the standing and sitting motions of an inverted pendulum-type assist robot, I-PENTAR. Whole-body motion based on redundant control that takes positional control of a composite center of gravity(CCoG) and a wrist roller as goal tasks is adopted. Using the motion control, motion planning of the robot can be described intuitively and in a simple manner. Compliance motion of a manipulator by force control of a wrist roller is adopted to move the position of CCoG and to maintain the robot's stability when the wrist roller contacts with the ground, which is an important factor in successfully achieving a sitting motion. Based on this motion control, standing and sitting motion planning is also proposed, which considers the stability and the operational time efficiency of the process. The proposed control method and motion planning were tested experimentally with I-PENTAR, and it was confirmed that standing and sitting motions were achieved stably in a short time period.**

I. INTRODUCTION

Many robots have been developed to provide physical assistance to humans through various activities such as delivery of objects and cleaning. It is essential that these robots not olny provide these services efficiently but also operate with a high degree of safety- they must perform their tasks without causing any injury. However, these two functions (providing efficient service and ensuring safety) have characteristics that are counterproductive and it is difficult to reconcile them. A robot with an inverted pendulum mobile platform has many features that suit its use for human support; it has high work capability using its own weight, is very mobile since it has a mechanically small footprint and does not need a caster, and its simple sutructure makes it lightweight.

Many studies on wheeled inverted pendulum-type robots focus on improving their mobility for activities, such as running, steering, and following a trajectory [1]– [13]. Yamafuji [1] [2] [3] proposed a wheeled inverted pendulum-type robot and realized stable traveling with it; Matsumoto [4] [5] examined a robot's stable travel by estimating its attitude using only internal sensors on a flat road as well as on an inclined path. Ha and Yuta [6] [7] developed an inverted pendulum mobile robot that could traverse an indoor environment with high mobility and robustness. However, few studies have been conducted to realize mobility combined with executing tasks. Matsumoto [14] realized a cooperative transportation task between two wheeled inverted pendulum robots using an observer to estimate external force and acting force. Bryan [15] proposed a pushing task that uses the robot's dynamic stability. Most recently, humanoid-type robots with an inverted pendulum mobile platform have been proposed that provide powerful mobility and limited manipulation tasks [16] [17], or the ability to make human-friendly gestures [18].

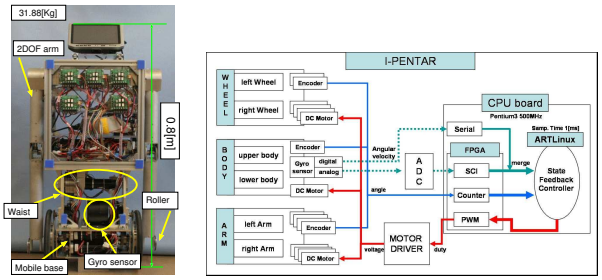

(a) Appearance (b) Control system

Fig. 1. Inverted pendulum-type assist robot, I-PENTAR

TABLE I
GENERAL SPECIFICATIONS OF I-PENTAR

Size	[m]	900 [H] × 340 [W] × 210 [D]
Weight	[kg]	32
DOF		Mobile (2), Arm (4), Waist (1)
CPU		Pentium3 500 [Mhz]
Sensor		Gyro sensor(1), Encoder(9)
Motor		DC motor(9)
Interface(Inner)		FPGA(PC104), VGA monitor-1
OS		ARTLinux(Sampling time:1 [ms])

The final goal of this study is to develop a robot assistant that provides high safety and affords good work ability, using a wheeled inverted pendulum mechanism. It should realize various motions, such as standing and sitting, picking an object up from the ground, and lifting a heavy object. These tasks require bending motions using a waist joint similar to that of a human. This has not been available with previous inverted pendulum robots.

In this paper, we briefly introduce the proposed Inverted PENdulum-Type Assistant Robot–(I-PENTAR) and its basic control, and then focus on stable and path-efficient standing and sitting motions. Standing and sitting motions are essential if the inverted pendulum-type assit robot is to be a practical one. The robot must frequently change from a static to a dynamic stable state for conducting various tasks, and must move safely in both states.

II. INVERTED PENDULUM-TYPE ASSISTANT ROBOT

A. I-PENTAR

Figure 1(a) shows the prototype robot developed in this study, I-PENTAR, and Table I describes its general speci-

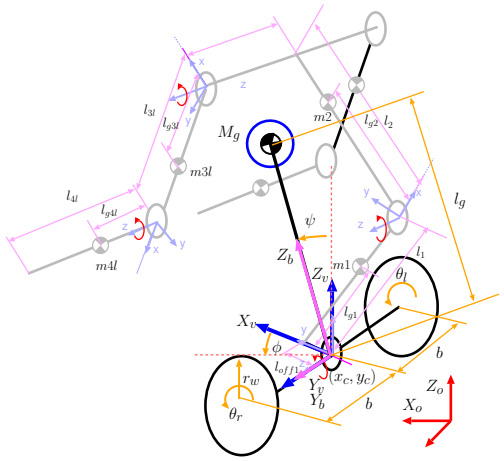

Fig. 2. A robot model

fications. I-PENTAR consists of a body with a waist joint, two low-powered and lightweight arms, and a two-wheeled inverted pendulum-type mobile platform. It adopts a double motor method for its mobile platform, which actuates a wheel with two motors to reduce the effect of backlash in the balancing controls, and to increase the platform's power. The lower body shares an axis with the wheel and freely rotates about the axis, thereby realizing an inverted pendulum mechanism. The body is divided into lower and upper parts by a waist joint, and a rate gyro sensor located in the lower body detects the inclination angle of the composite center of gravity(CCoG) with respect to ground. An mechanical stop is placed at the elbow, and a wheel roller adhered to the tip of the manipulator assists standing and sitting. The internal signal flow of I-PENTAR is showen in Fig.1(b). The control and sensor signals between the parts and a CPU board are interfaced via an FPGA board with 1 [ms] sampling time.

B. Inverted mobile control

Basic inverted mobile control is described in brief. Figure 2 shows a model of I-PENTAR. If the forward position, steering angle, and inclination angle of the CCoG are x_v, ϕ, ψ, respectively, the motion equations, considering non-holonomic constraints of the mobile platform, can be expressed as [19]

$$\hat{\boldsymbol{M}}\dot{\boldsymbol{\nu}} + \hat{\boldsymbol{H}}(\boldsymbol{\nu}, \dot{\boldsymbol{\nu}}) + \hat{\boldsymbol{V}}\boldsymbol{\nu} + \hat{\boldsymbol{G}} = \hat{\boldsymbol{E}}\boldsymbol{\tau} \tag{1}$$

where $\hat{\boldsymbol{M}}(\boldsymbol{q}) \in R^{6\times6}$ is the inertia matrix, $\hat{\boldsymbol{H}}(\boldsymbol{q}, \dot{\boldsymbol{q}}) \in R^{6\times1}$ is Coriolis and centrifugal forces, $\hat{\boldsymbol{V}} \in R^{6\times1}$ is the viscous coefficient matrix, $\hat{\boldsymbol{G}} \in R^{6\times1}$ is the gravity force, $\hat{\boldsymbol{E}}\boldsymbol{\tau} \in R^{6\times1}$ is the control torque, and $\boldsymbol{\nu}$ is $[\dot{x}_v\ \dot{\phi}\ \dot{\psi}]^T$.

In this study, we adopt a state feedback control method and determine the feedback gain by LQR(Linear Quderatic Regulator). Defining the generalized coordinate $\boldsymbol{q}_\nu = [x_v\ \phi\ \psi]$, then the system state variables can be represented as $\boldsymbol{x} = [\boldsymbol{q}_\nu\ \boldsymbol{\nu}]$. Linearizing the system with $\boldsymbol{x} \cong \boldsymbol{0}$, Eq. (1) can be simplified as

$$\hat{\boldsymbol{M}}\dot{\boldsymbol{\nu}} + \hat{\boldsymbol{V}}\boldsymbol{\nu} + \hat{\boldsymbol{G}} = \hat{\boldsymbol{E}}\boldsymbol{\tau}. \tag{2}$$

Note that each term in Eq. (2) has linearized components. Finally, a linear state equation is given as

$$\begin{aligned} \dot{\boldsymbol{q}}_\nu &= \boldsymbol{\nu} \\ \dot{\boldsymbol{\nu}} &= -\hat{\boldsymbol{M}}^{-1}(\hat{\boldsymbol{V}}\boldsymbol{\nu} + \hat{\boldsymbol{G}}) + \hat{\boldsymbol{M}}^{-1}\hat{\boldsymbol{E}}\boldsymbol{\tau} \end{aligned}$$

$$\dot{\boldsymbol{x}} = \boldsymbol{A}\boldsymbol{x} + \boldsymbol{B}\boldsymbol{u} \tag{3}$$

where $\boldsymbol{A} \in \boldsymbol{R}^{6\times6}$ and $\boldsymbol{B} \in \boldsymbol{R}^{6\times2}$. Here, a state feedback control law is introduced for the inverted mobile control as

$$\boldsymbol{u} = -\boldsymbol{K}\boldsymbol{x} \tag{4}$$

where $\boldsymbol{K}$ is a gain matrix calculated by LQR. Inputting the control torque, $\boldsymbol{u}$, obtained from Eq. (4) to the mobile platform realizes inverted mobile motion.

III. Strategy of Standing and Sitting Motions

A. Problem and approach

Two control shift processes are required for standing and sitting motions of I-PENTAR. First, it switches from a static stable state to a dynamic stable state, and then from a dynamic stable state to a static stable state.

For the former, robot's CCoG should be moved from a static stable position to a position that can be switched to dynamic control stably. A simple method is to move the CCoG by sliding the wrist roller on the ground in the direction of the wheel axis with the waist joint stationary [20]. However, this method has two demerits– it take a long time because the CCoG path is not a straight line but curves until just above the wheel axis, and the CCoG must move a long distance to achieve an upright standing posture because it is initially located low just above the wheel axis when balancing control starts. This also causes a large control parameter change, which worsens stability. Consequently, to improve operating efficiency and control stability, it is desirable to move the CCoG in a straight path to the highest possible position. This can be realized by directly controlling the position of the CCoG.

To switch from a dynamic stable to a static stable state, the CCoG should be moved into a stable area– an area where it could get support from wheels and wrist rollers– in a balancing state. We can consider controlling ψ directly, or using an inverse reaction of the CCoG to foward running control motion to move the CCoG [20]. In these cases, the wrist roller will not touch the ground because the robot can not lean over; thus the CCoG cannot be moved if it is in contact with the ground. However, if the wrist roller is off the ground when balancing control stops, it could generate a large impact force at the wrist roller due to the crash with the groud. This could possibly damage the manipulator joints. Moreover, since after switching the balancing control the CCoG is located at the edge of a stable area, vibrations from the stiffness of the mechanism and controller might overturn it. Consequently, it is desirable to locate the CCoG in a stable area but without causing a high impact load on the manipulator . This can be achieved by giving the manipulator a compliance motion and moving the CCoG with the wrist roller in constant contact with the groud.

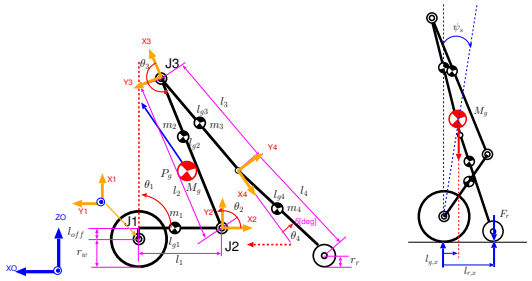

Fig. 3. (a) A 3-link model of I-PENTAR and (b) a contact model in a dynamic stable state.

This study solves these problems through whole-body motion control and a stable switching control method using force control of the wrist roller.

B. Whole-body motion with force control

1) Whole-body motion: The robot model for whole-body motion is shown in Fig. 3(a). For standing and sitting motions, the robot is considered as a 3-link and 3-joint model, with a fixed elbow joint in (X, Z) space, allowing the aplication of redundant control. In redundant control, a desired joint velocity vector, $\dot{\boldsymbol{\theta}}_{b,d}$, that can realize a first and second task is given by

$$\dot{\boldsymbol{\theta}}_{b,d} = \boldsymbol{J}_1^{+}\dot{\boldsymbol{P}}_1 + (\boldsymbol{I} - \boldsymbol{J}_1^{+}\boldsymbol{J}_1)\tilde{\boldsymbol{J}}_2^{+}(\dot{\boldsymbol{P}}_2 - \boldsymbol{J}_2\boldsymbol{J}_1^{+}\dot{\boldsymbol{P}}_1) \quad (5)$$

where $\dot{\boldsymbol{P}}_1$, $\dot{\boldsymbol{P}}_2$ are the task velocities for a first and second task, respectively, $\boldsymbol{J}_1$, $\boldsymbol{J}_2$ are Jacobian matrixes in each task, and $\tilde{\boldsymbol{J}}_2$ is $\boldsymbol{J}_2(\boldsymbol{I}-\boldsymbol{J}_1^{+}\boldsymbol{J}_1)$. In standing and sitting motions, the desired velocity of the CCoG, $\dot{\boldsymbol{P}}_{G,d}$, and the desired velocity of the wrist roller, $\dot{\boldsymbol{P}}_{r,d}$, are selected for the tasks; they are given as

$$\dot{\boldsymbol{P}}_{G,d} = \boldsymbol{K}_G(\boldsymbol{P}_{G,d} - \boldsymbol{P}_G), \quad (6)$$

$$\dot{\boldsymbol{P}}_{r,d} = \boldsymbol{K}_r(\boldsymbol{P}_{r,d} - \boldsymbol{P}_r) \quad (7)$$

where $\boldsymbol{K}_G$ and $\boldsymbol{K}_r$ are gain matrixes that adjust the convergence speed to a desired position. By substituting both desired velocities appropriately to $\dot{\boldsymbol{P}}_1$ and $\dot{\boldsymbol{P}}_2$ in Eq. (5) according to the motion situations, a desired joint velocity vector for whole-body motion can be obtained. Consequently, it is possible to realize standing and sitting motions by planning a suitable path for the CCoG and the wrist roller.

2) Compliance motion: Figure 3(b) shows the robot model with its wrist roller contacting the ground in a dynamic stable state. In this case, the relation between the contact force of the wrist roller against the ground and joint torque is given as

$$\boldsymbol{\tau} = \boldsymbol{J}_r^{T}\boldsymbol{F}_r, \quad (8)$$

where the torque of wheel, $\bar{\tau}_w$, is defined as

$$\bar{\tau}_w = [\boldsymbol{J}_{r,(11)}\ \boldsymbol{J}_{r,(21)}][0\ \boldsymbol{F}_{r,(z)}]^{T} = \boldsymbol{J}_{r,(21)}\boldsymbol{F}_{r,(z)} \quad (9)$$

where $\boldsymbol{\tau} \in R^3$ is the joint torque, $\boldsymbol{J}_r \in R^{2\times 3}$ is the Jacobian of the wrist roller, $\boldsymbol{F}_r \in R^2$ is the contact force between the wrist roller and the ground, $\boldsymbol{J}_{r,(ij)}$ represents the (i,j) component of $\boldsymbol{J}_r$, and $\boldsymbol{F}_{r,(z)}$ represents the (z) component of $\boldsymbol{F}_r$. $\boldsymbol{J}_{r,(12)}$ has the same value as the x position of the wrist roller.

From Eq. (1), $\bar{\tau}_w$ can be also expressed as

$$\bar{\tau}_w = M_g l_g \sin\psi_s g \quad (10)$$

where M_g is the robot's total mass, l_g is the distance between the origin of the wheel axis and the CCoG, ψ_s is ψ of a contact situation, and g is the gravitational acceleration. Consequently, from Eqs. (9) and (10), the following equation can be derived.

$$\boldsymbol{F}_{r,(z)} = \frac{M_g l_g \sin\psi_s g}{\boldsymbol{J}_{r,(21)}}. \quad (11)$$

Equation (11) shows how much contact force is generated when ψ is ψ_s, and the contract force can be estimated by ψ_s.

To realize compliance motion by the manipulator, consider the following equation

$$\hat{\boldsymbol{P}}_{r,d} = \boldsymbol{P}_{r,d} + \boldsymbol{K}_f(\boldsymbol{F}_{r,d} - \boldsymbol{F}_r) \quad (12)$$

where $\hat{\boldsymbol{P}}_{r,d}$, $\boldsymbol{P}_{r,d}$ are the final desired position and desired position of the wrist roller, respectively, $\boldsymbol{F}_{r,d}$ is the desired contact force, and $\boldsymbol{K}_f$ is the stiffness gain matrix. The equation modifies the desired position of the wrist roller according to the contact force. Consequently, the manipulator is able to act as a spring by setting $\boldsymbol{F}_{r,d} = \boldsymbol{0}$ according to $\boldsymbol{F}_r$ which is estimated by Eq. (11) or measured by a force sensor on the wrist roller.

3) Control torque: The robot is controlled by the following control law, which uses the the desired joint velocity and the desired state values. These are given as

$$\boldsymbol{\tau}_w = -\boldsymbol{K}_w(\boldsymbol{x} - \boldsymbol{x}_d) + \frac{1}{2}\begin{bmatrix} \bar{\tau}_w \\ \bar{\tau}_w \end{bmatrix} \quad (13)$$

$$\boldsymbol{\tau}_b = \boldsymbol{K}_{b,p}(\tilde{\boldsymbol{\theta}}_{b,d} - \boldsymbol{\theta}_b) - \boldsymbol{K}_{b,v}\dot{\boldsymbol{\theta}}_b \quad (14)$$

where $\boldsymbol{\tau}_w$ is the torque of the wheel joint, $\boldsymbol{\tau}_b$ is the torque of the waist and shoulder joints, and $\boldsymbol{K}_*$ is each control gain. $\bar{\tau}_w$ is the feedforward wheel torque when $\psi = \psi_s$, and $\tilde{\boldsymbol{\theta}}_{b,d}$ is the integrated value from the vector composed of the second and third components of $\dot{\boldsymbol{\theta}}_{b,d}$ in Eq. (5). Note that Eq. (13) can be applied to both static stable and dynamic stable states by changing the value of $\boldsymbol{K}_w$. For balancing control, normal state feedback control is applied to the wheel joint using control gain $\boldsymbol{K}_w$ obtained by the LQR method. For a static stable state, however, the control related to ψ is not necessary, and the related gain is set to 0. The sign of the gain related to x_v is opposite that in balancing control. The total control block is shown in Fig. 4.

IV. Standing and Sitting Motion Planning

A. Standing motion planning

Standing motion is divided into three steps; assumed a posture for dynamic balancing control (Step 1), switch to

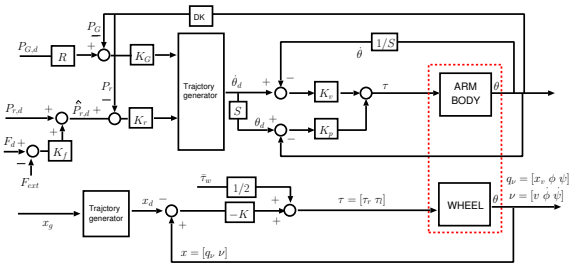

Fig. 4. Control block of I-PENTAR

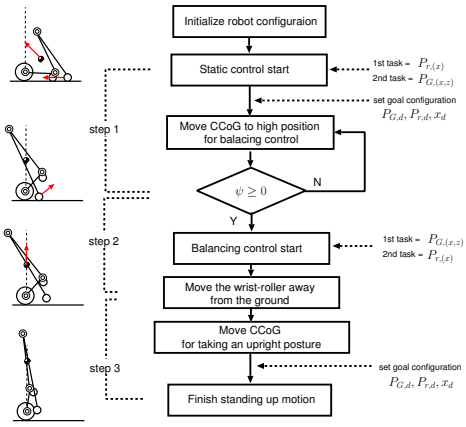

Fig. 5. Flowchart of the standing motion

dynamic balancing control(Step 2), and assume an upright standing posture (Step 3). The flowchart for the standing motion is shown in Fig. 5.

Step 1: Assume a posture for dynamic balancing control. In step 1, the robot moves the CCoG from the sitting posture to a position where it can stably switch to dynamic balancing control; $\psi = 0$. To execute the motion stably and quicky, the CCoG most move to a higher position above the wheel axis following a straight path. This can be achieved by directly controlling the x, z position of the CCoG. For an inverted pendulum-type robot, such as I-PENTAR, J_1 is a free joint and should be rotated with reaction force from the ground. Therefore, the z position of the wrist roller should be controlled simultaneously. Consequently, the z position of the wrist roller should be chosen as the first task and the x, z position of the CCoG as the second task in redundant control. Thus, in Eq. (5)

$$\dot{\boldsymbol{P}}_1 = \boldsymbol{K}_{r,(z)}(\boldsymbol{P}_{r,d,(z)} - \boldsymbol{P}_{r,(z)}), \quad (15)$$

$$\dot{\boldsymbol{P}}_2 = \boldsymbol{K}_G(\boldsymbol{P}_{G,d} - \boldsymbol{P}_G). \quad (16)$$

When the robot is in motion, the wheels are controlled to maintain their initial position.

Figure 6 shows the realizable and switchable areas of the CCoG for I-PENTAR. As shown in the figure, I-PENTAR can locate the CCoG from a minimum of 0.3[m] to a maximum of 0.38[m] from the origin of the wheel axis, wherein the angle of the joints are $(-52, 93, 170)$[deg] and $(-29, 51, 160)$[deg] respectively.

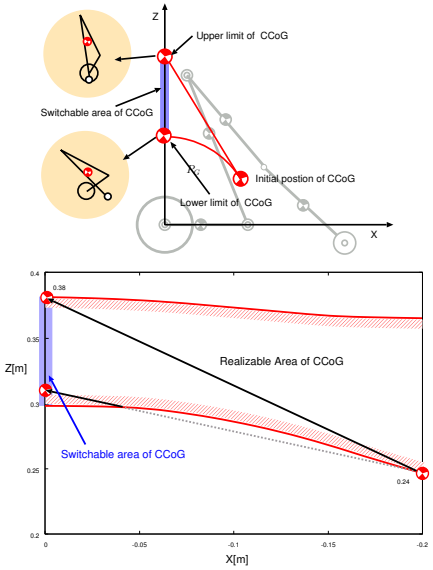

Fig. 6. Realizable and switchable areas of CCoG for I-PENTAR

Step 2: Switch to dynamic balancing control. When the CCoG reaches above the wheel axis ($\psi = 0$), the control switches to dynamic balancing control. After switching, the x, z position of the CCoG is set to the first task, and the x position of the wrist roller becomes the second task, as follows.

$$\dot{\boldsymbol{P}}_1 = \boldsymbol{K}_G(\boldsymbol{P}_{G,d} - \boldsymbol{P}_G), \quad (17)$$

$$\dot{\boldsymbol{P}}_2 = \boldsymbol{K}_{r,(x)}(\boldsymbol{P}_{r,d,(x)} - \boldsymbol{P}_{r,(x)}). \quad (18)$$

Note that the x position of the wrist roller is chosen here to keep consistent motion control in step 3. Since grounding the wrist roller disturbs balancing control, the wrist roller must lose contact with the ground as quickly as possible. To realize this, the shoulder joint rotates in the direction that takes the wrist roller away from the ground. The desired value of x_v and ϕ is set to 0 to keep the wheels at the present position.

Step 3: Assume an upright standing posture. In this step, the robot stretches its waist and assumes upright standing posture. This motion can be achieved by raising the z position of the CCoG gradually while maintaining the x position above the wheel axis. During the motion, although it is not necessary to control the z position of the wrist roller, it is desirable to locate the x position close to the body. Accordingly, in this step, the position control of the CCoG is selected as the first task and the x position control of the wrist roller is the second task, as in step 2.

B. Sitting Motion Planning

Sitting motion planning is also divided into three steps; ground the wrist roller (step 1), switch control to static stable

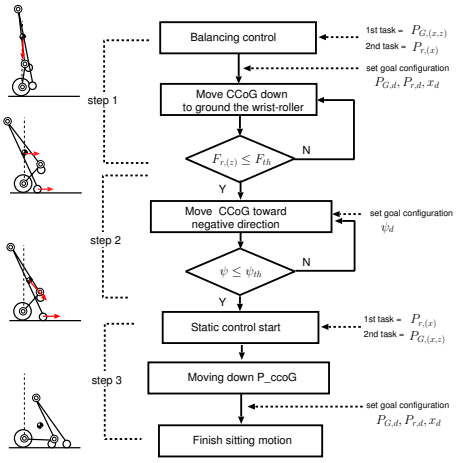

Fig. 7. Flowchart of the sitting motion

state (step 2), and assume a sitting posture (step 3). Figure 7 shows a flowchart of sitting motion.

Step 1: Ground the wrist roller. In step 1, the robot grounds the wrist roller from an upright standing posture. This motion can be achieved by lowering the z position of the CCoG while maintaining robot's balance. The wrist roller approaches the ground and the waist joint is automatically bent. The wrist roller must be located behind the wheel axis ($\boldsymbol{P}_{r,(x)} < 0$) for realizing step 2. Therefore, position control of the CCoG is the first task and the x position control of the wrist roller is the second task similar to step 3 for the standing motion.

Step 2: Switch to static stable state control. In this step, the robot switches dynamic balancing control to static stable state control. When there is no external force, the robot swings back and forth in a regular periodic motion to maintain its balance during dynamic balancing control; therefore, it may fall down (forward) if control is switched when $\psi > 0$. To avoid falling down, switching should begin after moving the CCoG behind the wheel axis ($\psi < 0$). Moreover, the impact force generated between the wrist roller and the ground should be supressed. To accommodate both of these critical conditions, the method that directly moves the CCoG backward when the wrist roller contacts the ground, by giving the manipulator a compliance function, is adopted. The following tasks are given in this step.

$$\dot{\boldsymbol{P}}_1 = \boldsymbol{K}_G(\boldsymbol{R}\boldsymbol{P}_{G,d} - \boldsymbol{P}_G) \quad (19)$$

$$\dot{\boldsymbol{P}}_2 = \boldsymbol{K}_{r,(z)}(\hat{\boldsymbol{P}}_{r,d,(z)} - \boldsymbol{P}_{r,(z)}). \quad (20)$$

By switching the balancing control when ψ reaches a threshold by the above method, the robot can takes a posture of stably supported by the wheels and the manipulators without occuring a forward falling and generating large impact force.

Step 3: Assume a sitting posture. In this step, the robot shifts to the same sitting posture as its initial posture. This motion can be achieved by reversing step 1 from the standing motion planning. By completing this motion, the robot finally attains a seated posture, stably supported by wheels and a caster.

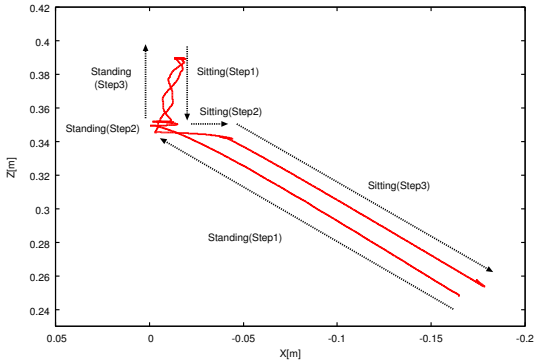

(a) Position of CCoG

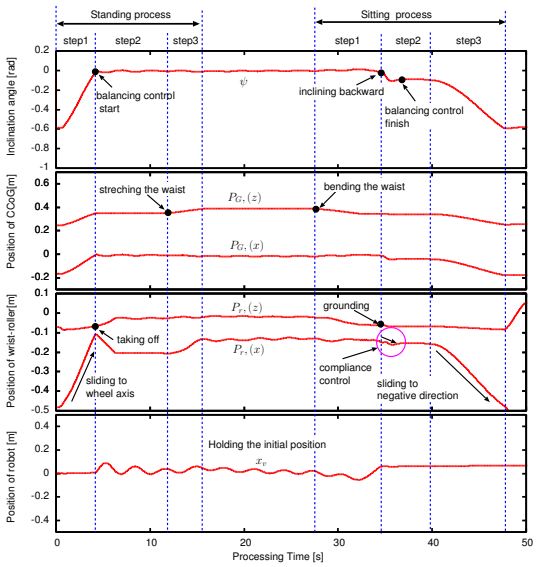

(b) ψ, P_G, P_r, x (from top)

Fig. 8. Experimental results of standing and sitting motions

V. Experiment

Experiments with standing and sitting motions were conducted to confirm the effectiveness of the proposed motion control and planning, using I-PENTAR. In the experiment, the robot begins moving from a static stable posture, supported by a caster and wheels. This is a deep seated posture with the waist bent. It moves to an upright standing posture with the waist joint stretched. Finally, it returns to the initial sitting posture. The experimental results are shown in Fig. 8. Figure 8(a) shows a profile of the CCoG positions and Fig. 8(b) shows a profile of ψ, $\boldsymbol{P}_G$, $\boldsymbol{P}_r$, x_v from the top.

The position of the CCoG in the initial posture is (-0.181, 0, 0.236)[m]. In initiating the standing motion, the CCoG moves directly to a goal position (0, 0, 0.35)[m] through simultaneous motion of the wrist roller and the waist joint (Standing, Step 1). As shown in Fig. 8(a), the CCoG moves directly (in a straight line) from the initial position to the

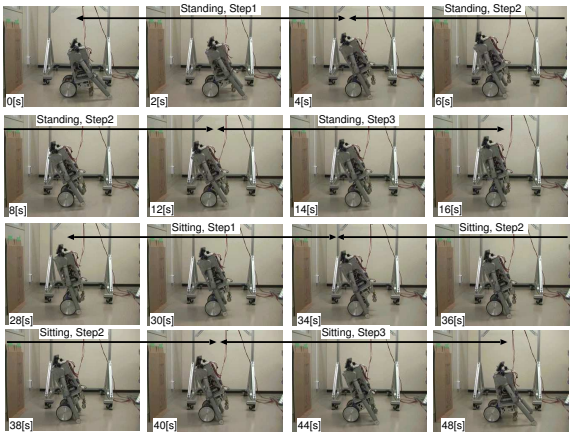

Fig. 9. Snapshots of the experimental results of standing and sitting motions by I-PENTAR

goal position. When $\boldsymbol{P}_{G,(x)}$ reaches 0 ($\psi = 0$), through Step 1, motion control switches to dynamic balancing control, and the robot rapidly removes the wrist roller from the ground (Standing, Step 2). Then, the robot moves the CCoG to (0, 0, 0.39) [m], while $\boldsymbol{P}_{r,(x)}$ approaches -0.15[m] and completes the standing motion by assuming an upright standing posture(Standing, Step 3). $\boldsymbol{P}_G$ inclines as the z position increases in step 3 (standing motion), as shown in Fig. 8(a), due to an estimation error in the CCoG position.

In sitting motion, the robot holds $\boldsymbol{P}_{r,(x)}$ at -0.15[m] and lowers $\boldsymbol{P}_{G,(z)}$ until the wrist roller touches ground (sitting, Step 1). When the output of the wrist roller's force sensor becomes -2[N], the robot judges that the wrist roller is touching the ground and leans the CCoG in a negative direction. The reason that the threshold of contact force is set to not 0[N] but -2[N] is to prevent misjudging due to noise. After grounding, the manipulator acts through compliance motion, according to the force generated between the wrist roller and the ground. The goal contact force in compliance motion is set to 0[N]. Figure 8(b) shows that the CCoG and $\boldsymbol{P}_{r,(x)}$ moves in a negative direction as a result of the compliance motion. When ψ reaches a threshold angle, -1[deg], the robot halts balancing control and initiates static stable control (sitting, Step 2), and finally returns to the initial position (sitting, Step 3). The complete time for the operation is 16[s] for standing motion and 20[s] for sitting motion. This may be shortened by increasing the operating speed. Snapshots from the experimental video clips are shown in Fig. 9

The experimental results confirmed that an inverted pendulum-type robot, such as I-PENTAR, can achieve standing and sitting motions stably and efficiently by applying the proposed motion control and planning.

VI. Conclusion

This study described the stable and path-efficient standing and sitting motions of an inverted pendulum-type robot, I-PENTAR. To realize the motion, whole-body motion control, including force control of the wrist roller, and standing and sitting motion planning were proposed. Applying the proposed method in experiments with I-PENTAR confirmed that the robot could successfully stand and sit. In future, we will improve the stability and speed of motion by considering dynamic effects of the robot.

References

[1] Kazuo Yamafuji, Takashi Kawamura,"Postural Control of a Monoaxial Bicycle", JRSJ, vol 7, no.4, pp. 74-79, 1988.

[2] Kazuo Yamafuji, Yasushi Miyakawa, Takashi Kawamura, "Synchronous Steering Control of a Parallel Bicycle", JSME, vol. 55, no. 513, pp. 1229-1234, 1989.

[3] Tsuyoshi Yasui, Kazuo Yamafuji, "Motion control of the Parallel Bicycle-Type Mobile Robot which is composed of a Triple Inverted pendulum(1st Report, Stability Control of Standing Upright, Ascending and Descending of Stairs", JSME, vol. 57(C), no. 538, pp. 114-119, 1991.

[4] Osamu Matsumoto, Shuuji Kajita, Kazuo Tani, "Estimation and Control of Attitude of a Dynamic Mobile Robot Using Internal Sensors", JRSJ, vol. 8, no. 5, pp. 37-46, 1990.

[5] Osamu Matsumoto, Shuuji Kajita, kazuo Tani, "Attitude Estimation of the Wheeled Inverted Pendulum Using Adaptive Observer", 19th Annual Conference of RSJ, pp. 909-910, 1991.

[6] Yunsu Ha, Shinichi Yuta, "Trajectory Tracking Control for Navigation of Self-Contained Mobile Inverse Pendulum", Proc. of the 1994 IEEE/RSJ int. Conf. on Intelligent Robotics and Systems, pp. 1875-1882, 1994.

[7] Yunsu Ha, Shinichi Yuta, "Indoor Navigation of an Inverse Pendulum Type Autonomous Mobile Robot with Adaptive Stabilization Control System", 4th International Symposium on Experimental Robotics (ISER) '95, pp. 331-336, 1995-06.

[8] Felix Grasser, Aldo D'Arrigo, Silvio Colombi, "JOE: A Mobile, Inverted Pendulum", IEEE Trans. on Industrial Electronics, vol. 49, no. 1, 2002.

[9] Kaustubh Pathak, Jaume franch, Sunil K. Agrawal, "Velocity Control of a Wheeled Inverted Pendulum by Partial Feedback Linearization", IEEE Conference on Decision and Control, pp. 3962-3967, 2004.

[10] Kaustubh Pathak, Jaume franch, Sunil K. Agrawal, "Velocity and Position Control of a Wheeled Inverted Pendulum by Partial Feedback Linearization", IEEE Trans. on Robotics, vol. 21, no.3, pp. 505-512, 2005.

[11] Yeon Hoon Kim, Dong-Yeon Lee, Soo Hyun Kim, Yoon Keun Kwak, "Emotional Action Simulation of 2 Wheeled Inverted Pendulum Mobile Robot", The IASTED Conference on Modeling, Simulation, and Optimization, pp. 266-271, 2003.

[12] Y Kim, S H Kim, and Y K Kwak, "Improving driving ability for a two-wheeled inverted-pendulum-type autonomous vehicle", Proc. of the Institution of Mechanical Engineers, Part D: Journal of Automobile Engineering, vol. 220, no. 2, pp. 165 - 175, 2005.

[13] Michael Baloh, Michael Parent, " Modeling and Model Verification of an Intelligent Self-Balancing Two-Wheeled Vehicle for an Autonomous Urban Transportation System", The Conference on Computational Intelligence, Robotics, and Autonomous Systems, pp. 1-7, 2003.

[14] Osamu Matsumoto, Shuuji Kajita, kazuo Tani, "Cooperative Behavior of a Mechanically Unstable Mobile Robot for Object Transportation", JSME, vol.64(C), no. 628, pp. 164-171, 1998.

[15] Bryan J.Thibodeau, Patrick Deegan, Roderic Grupen, "Static Analysis of Contact Forces With a Mobile Manipulator", Proc. ICRA, pp. 4007-4012, 2006.

[16] EMIEW, Hitachi, Ltd., http://www.hqrd.hitachi.co.jp/merl/emiew.cfm

[17] Robin, Robo3, Ltd., http://www.robo3.com/maink.htm

[18] Robovie 3, ART, Ltd., http://www.irc.atr.jp/productRobovie/robovie-2.html

[19] SeongHee Jeong, Takayuki Takahashi, " Wheeled inverted pendulum type assistant robot: Design concept and mobile control", Proc. of the 13th International Conference on Advanced Robotics, pp. 730-735, 2007.

[20] SeongHee Jeong, Takayuki Takahashi, "Wheeled inverted pendulum type Assistant robot: Inverted Mobile, Standing, and Sitting Motions", Proc. of the 2007 IEEE/RSJ International Conference on Intelligent Robots and Systems, pp. 1932-1937, 2007.